DocuServe

Electronic Delivery Cover Sheet

Caltech Library Services

Phys. Status Solidi A **210,** No. 2, 255–260 (2013) / **DOI** 10.1002/pssa.201228690

physica status solidi a
www.pss-a.com
applications and materials science

Solar cell efficiency enhancement via light trapping in printable resonant dielectric nanosphere arrays

Jonathan Grandidier*[,1], Raymond A. Weitekamp[1,2], Michael G. Deceglie[1], Dennis M. Callahan[1], Corsin Battaglia[3], Colton R. Bukowsky[1], Christophe Ballif[3], Robert H. Grubbs[2], and Harry A. Atwater[1]

[1] Thomas J. Watson Laboratories of Applied Physics, California Institute of Technology, Pasadena, CA 91125, USA
[2] Arnold and Mabel Beckman Laboratories of Chemical Synthesis, Division of Chemistry and Chemical Engineering, California Institute of Technology, Pasadena, CA 91125, USA
[3] Ecole Polytechnique Fédérale de Lausanne (EPFL), Institute of Microengineering (IMT), Photovoltaics and Thin Film Electronics Laboratory, 2000 Neuchâtel, Switzerland

Received 5 October 2012, revised 24 October 2012, accepted 24 October 2012
Published online 22 November 2012

Keywords amorphous silicon, nanospheres, photonic crystal, photovoltaics, resonant dielectric structures, solar cells

* Corresponding author: e-mail jgrandid@caltech.edu, Phone: +1 626 395 2193, Fax: +1 626 844 9320

Resonant dielectric structures are a promising platform for addressing the key challenge of light trapping in thin-film solar cells. We experimentally and theoretically demonstrate efficiency enhancements in solar cells from dielectric nanosphere arrays. Two distinct amorphous silicon photovoltaic architectures were improved using this versatile light-trapping platform. In one structure, the colloidal monolayer couples light into the absorber in the near-field acting as a photonic crystal light-trapping element. In the other, it acts in the far-field as a graded index antireflection coating to further improve a cell which already included a state-of-the-art random light-trapping texture to achieve a conversion efficiency over 11%. For the near-field flat cell architecture, we directly fabricated the colloidal monolayer on the device through Langmuir–Blodgett deposition in a scalable process that does not degrade the active material. In addition, we present a novel transfer printing method, which utilizes chemical crosslinking of an optically thin adhesion layer to tether sphere arrays to the device surface. The minimally invasive processing conditions of this transfer method enable the application to a wide range of solar cells and other optoelectronic devices.

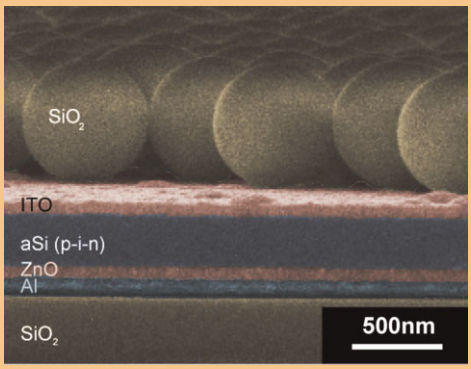

False-color SEM image of an amorphous silicon solar cell with resonant spheres on top.

1 Introduction Thin-film photovoltaic (PV) cells have a number of key advantages over wafer-based devices, including improved reduced active material usage, weight and cost [1]. However, the corresponding loss in optical absorption often reduces the cell efficiency, mitigating the advantages of thin-film absorber cells. Dielectric texturing [2] and optimized antireflection coatings [3] are commonly employed in silicon (Si) wafer-based PVs to increase light absorption. A textured active material increases light trapping, however, the large-scale features that are commonly employed for crystalline Si solar cells cannot be employed for thin-film cells, which often have total thicknesses of the order of the optical wavelength. As well, physical modification of the absorber layer by patterning or etching can result in degraded material quality and thus reduced carrier collection efficiency [4]. It is therefore desirable to develop a texture process for thin-film cells that does not in any way compromise the electronic performance

of the absorber, junction, and passivation layers. Recently, a number of innovative solar cell light-trapping methods have been proposed including some using spherical schemes. Plasmonic structures [5–7], gratings [8], photonic crystals (PC) [9], Mie resonators [10, 11], and dielectric diffractive structures [12] have all been investigated as light-trapping elements. In this context, colloidally synthesized sphere arrays of resonant dielectric spheres are attractive because they are low loss and they do not affect or compromise solar cell electronic performance.

When sphere array layers are placed at wavelength-scale distances from a thin-film cell, the resonant modes in the spheres leak into the absorber layer [13], increasing absorption. We have previously reported simulations which predict that a nanosphere array on top of a thin-film hydrogenated amorphous silicon (a-Si:H) or gallium arsenide solar cell can significantly increase both light absorption in the active layer [14, 15] and device efficiency [16]. Here, we report experimental results that are in good accord with the predictions from full field finite difference time domain (FDTD) optical simulations, and device physics simulations. Angle-resolved external quantum efficiency (EQE) measurements were performed and compared to rigorous coupled wave analysis (RCWA). Our experimental results support the light-trapping mechanism suggested by simulation.

2 Fabrication

2.1 Solar cell fabrication Amorphous silicon solar cells with an intrinsic absorber layer thickness of 250 nm were deposited in p–i–n sequence by plasma-enhanced chemical vapor deposition in an industrial KAI reactor with parallel plate configuration. More details can be found in Ref. [17]. The flat cell was deposited on an 80 nm thick sputtered aluminum back reflector covered by 70 nm of sputtered zinc oxide (ZnO). A 70-nm thick sputtered indium tin oxide (ITO) was used as transparent front electrode and efficient antireflection coating. The cells were patterned to $5 \times 5\,\mathrm{mm}^2$ by lift-off and SF_6 reactive ion etching.

2.2 Sphere deposition Experimentally, one of the main challenges to realizing such resonant nanosphere enhanced solar cells is in fabricating a large monolayer of closely packed spheres. Diffractive coupling occurs when the spheres are periodically arranged as a 2D colloidal crystal [18]. Hexagonally packed spheres of relatively uniform diameter offer an optimal geometry to enhance the efficiency in the cell via PC resonances. Many methods of colloidal crystal assembly can be found in the literature, including controlled evaporation [19], sedimentation [20], and spin coating. Compared to many other attempted techniques, we found Langmuir–Blodgett (LB) deposition [21] to yield the highest quality 2D colloidal crystals of silica spheres with diameters near visible wavelengths and to have the highest long-range order and lowest number of multilayer and gap defects. The trough we used is intended for samples of a few centimeter squares, but this technique has been extended to full wafers [22] and could potentially be scaled to PV module dimensions. We used uniform silica spheres from Polysciences Inc., with a nominal diameter of 700 nm. Our simulations indicated that this diameter yielded the highest photocurrent enhancement for a thin-film a-Si:H solar cell [23]. Other materials for the spheres such as polystyrene or TiO_2 are discussed in Ref. [23]. The spheres were functionalized with an aminopropyl silane, and deposited from a dilute suspension in 1:4 ethanol:dichloromethane, compressed on an acidic aqueous sub-phase. We found that the long-range order of the colloidal crystals was highly dependent on the pH of the sub-phase. We attribute this result to the electrostatic repulsion of the protonated RNH_3^+ ions on the functionalized sphere surface, which mitigate sphere–sphere attraction in the suspension. Reduced aggregation would account for the improved long-range order and reduced multilayer formation. For this study, we used a solution of $pH \approx 2.5$, corresponding to two drops of concentrated hydrochloric acid in 250 mL deionized water. Details of the surface functionalization and LB deposition parameters can be found in the Supporting Information (online at: www.pss-a.com).

Figure 1a depicts the LB process used to deposit a uniform monolayer array of silica nanospheres atop the thin-film a-Si:H solar cell. Scanning electron microscopy (SEM) as well as atomic force microscopy (AFM) images of the nanosphere array are shown in Fig. 1b and d. The influence of the separation between the sphere array and the active layer is discussed in Ref. [16]. The Fourier transform of a large-area SEM image of the nanosphere array yields an average periodicity of $\Lambda = 700$ nm. Because the spheres are closely

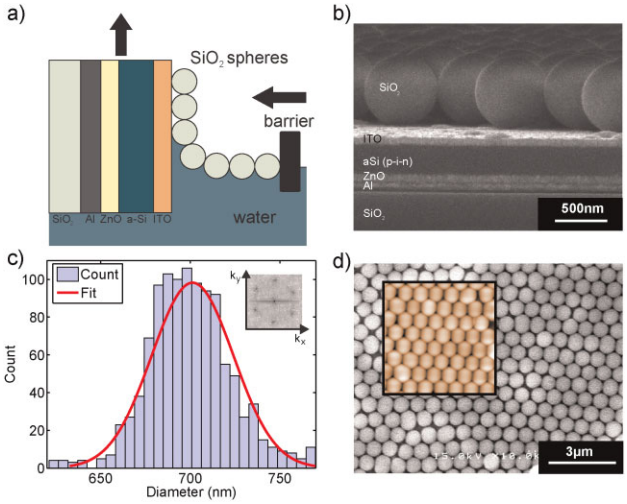

Figure 1 (online color at: www.pss-a.com) A silica colloidal monolayer on a solar cell. (a) Schematic of the sphere deposition on the solar cell using the Langmuir–Blodgett method. (b) SEM cross-section of the solar cell with resonant spheres on top. (c) Size distribution histogram of the spheres and the corresponding Gaussian fit. The inset displays a Fourier transform of an SEM image of the spheres. (d) SEM image with a corresponding AFM image as an inset (on the same scale).

packed, we assume that the average periodicity is equal to the average diameter of the spheres. From the direct space of an SEM image, we are able to estimate the sphere size distribution on a sample of about 1000 spheres using image analysis software (imageJ). We assume a Gaussian distribution for the sphere size, which fits the counted distribution relatively well (Fig. 1c).

3 Measurement and simulation

3.1 Normal incidence We measured the EQE of cells coated with dielectric nanospheres and repeated this measurement after removing the spheres from the surface (Fig. 2a) using a Q-tip and methanol. Since ITO does not dissolve in methanol, we do not expect this process to affect the optical or electrical properties of the solar cell. The coated cells showed broadband enhancement over the measured spectrum. Weighting the EQE by the AM1.5G solar spectrum gives, for the flat cell, a short circuit current density of 8.8 mA cm^{-2}, and for the cell coated with spheres 9.6 mA cm^{-2}, corresponding to a relative enhancement of 9.1%. Using an AM1.5G solar simulator, we performed white light current voltage measurements on five similar solar cells coated with spheres and with the spheres subsequently removed. The average relative enhancement for the efficiency is $7.0 \pm 1.8\%$, and $8.5 \pm 1.5\%$ for the short circuit current (J_{sc}), in good agreement with the measured EQE weighted by the AM1.5G solar spectrum. Figure 2b plots the current–voltage measurement for the solar cell demonstrating the highest efficiency enhancement, which is almost 10% from 4.39 to 4.81%. We were able to reproduce these current–voltage curves with full 3D finite element device physics simulations [16, 24], taking the generation rate as calculated via FDTD as input (see Supporting Information).

In order to analyze each of the features in the measured EQE, we first plot the result of the simulation for spheres of the median diameter, 700 nm, in Fig. 3b. We verified experimentally and theoretically [16] that the EQE is independent of the polarization at normal incidence. Several sharp and distinct peaks are observed in this simulation.

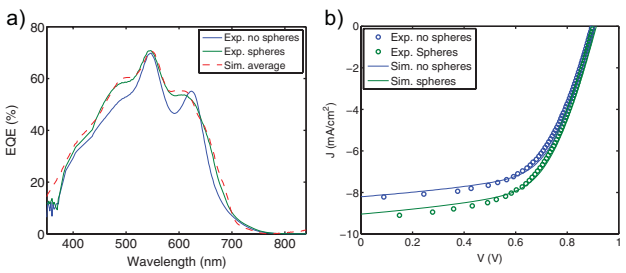

Figure 2 (online color at: www.pss-a.com) PV performance. (a) EQE measurement of the flat solar cell with and without dielectric spheres on top. The red dashed line corresponds to optical simulations (see Supporting Information) of a solar cell with spheres on top weighted by the average size distribution. (b) Current–voltage curve measured with an AM1.5G solar simulator and corresponding device physics simulation.

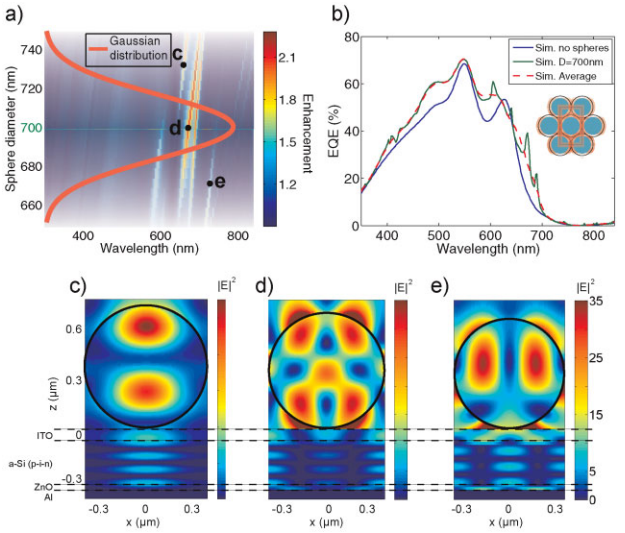

Figure 3 (online color at: www.pss-a.com) FDTD simulations of a resonant dielectric structure on a solar cell. (a) Map of the enhancement of the EQE of an a-Si:H solar cell with spheres over the EQE of the cell without spheres as a function of the wavelength for the different sphere diameters across the measured size distribution, and the Gaussian fit used to weight the individual simulations (in arbitrary units, taken from Fig. 1c). (b) Optically simulated EQE (see Supporting Information) for the PV structure with and without dielectric spheres on top. (c–e) For each labeled peak on (a): the electric field intensity in V^2 m^{-2} for a cross section at the middle of a sphere.

For three points on this plot, we plot the electric field intensity for a cross section at the middle of a sphere in the same plane as the polarization of the normal incident plane wave in Fig. 3c–e. It can be seen that numerous resonant modes exist within the experimental size distribution of the spheres, covering a broad range of wavelengths. To explain the entire experimental spectra, we must consider multiple optical coupling mechanisms that are possible with these wavelength scale resonant structures, depending on the region of the spectrum we consider. For wavelengths approximately between 350 and 550 nm, we observe EQE enhancement that is relatively independent of the size distribution of the spheres. We attribute this enhancement mainly to the Fabry–Perot resonance formed by the array of spheres as similar features are observed in a homogeneous slab with the volume-weighted refractive index of the spheres in air (Fig. S1, see Supporting Information). We attribute the enhancement in the spectral range between 550 and 750 nm to coupling to in-plane leaky modes of the 2D PC bandstructure, greatly broadened due to the experimental size distribution of the spheres. To explain this enhancement, we simulate 21 cases for sphere diameters varying between 650 and 750 nm using the observed size distribution range shown in Fig. 1c. Each simulation assumes an infinite array of spheres with periodic boundary conditions. In order to account for the experimentally measured distribution of the sphere size, we weighed the

set of simulations by the Gaussian distribution represented in Fig. 1c. The resonant features of the experimental spectrum and the weighted average spectrum are very well matched (Fig. 2a). From this analysis, we conclude that the features in the experimental EQE spectra from 550 to 750 nm are associated with the excitation of resonant modes of the colloidal monolayer [14] and thus that the observed enhancement in this spectral range is due to leaky PC modes. Prior literature also attributes these resonant features to both PC modes and Mie resonances [25] or whispering gallery modes [14]. This result demonstrates that the excitation of modes within a low loss dielectric resonant structure can have a significant impact on the EQE enhancement of a solar cell. Reflection measurements of a 2D colloidal crystal on a Si (Fig. S2, see Supporting Information) wafer support the proposed mechanism of enhancement (Figs. S3 and S4, see Supporting Information).

3.2 Angle dependence We then measured the angle dependence (Fig. S6, see Supporting Information) of the EQE in both TE and TM polarizations and plot in Fig. 4a the average relative EQE enhancement for angles varying between 0° and 70°. The observed EQE enhancement bands account for the variation of the structure's resonances as a function of the angle of incidence. In order to evaluate the performance of the PV structure, we interpolated angle-resolved data [26] of the incident solar energy on a sunny day to match the resolution of our EQE measurements corresponding to Fig. 4a. Figure 4b shows the equivalent simulated plot using RCWA for 700 nm diameter spheres. We then compare the angle-dependent photocurrent generated by a flat cell and a cell with spheres (Fig. 4c) and calculate the relative short circuit current enhancement due to the colloidal crystal (Fig. 4d). It varies between 5.0% (at 55°) and 8.9% (at 0°) with an average of 6.3% through the day. The strongest enhancement is observed at normal incidence. The relatively angle-independent enhancement is a promising result; it demonstrates that these resonant dielectric structures can couple direct and scattered sunlight throughout the day.

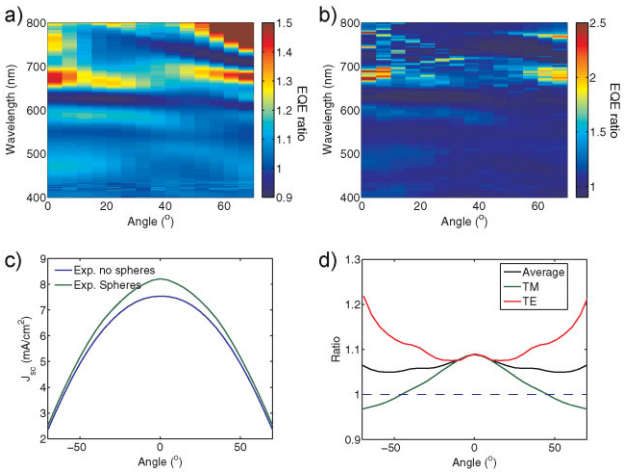

Figure 4 (online color at: www.pss-a.com) Angle resolved analysis. (a) Angle resolved measurement of the EQE enhancement, averaged over TE and TM polarizations. Calculated from the ratio of the sphere coated EQE to the flat cell EQE. (b) Corresponding simulation using RCWA for the median size sphere diameter (700 nm). (c) J_{sc} generated by the active material for the case with and without spheres. TE and TM polarization were averaged to account for the unpolarized nature of solar radiation. Tabulated data of solar irradiance was used to weight the measured absorption [26]. (d) Relative enhancement over the flat solar cell as a function of the incident angle for TE, TM and averaged polarizations.

4 Effective ARC on a state-of-the-art solar cell

Finally, we demonstrate performance enhancement from a sphere array on an a-Si:H solar cell with a state-of-the-art architecture [27] and a high initial efficiency of 10.9%. This solar cell consists of a rough ZnO/a-Si:H/ZnO structure deposited on glass (Fig. 5a). It was deposited on a 2-μm thick transparent ZnO front electrode grown by low-pressure chemical vapor deposition featuring the characteristic naturally textured pyramidal surface morphology [27]. The ZnO surface was treated with argon plasma to optimize the morphology for cell deposition. A 2.5-μm thick transparent ZnO layer was used as a back electrode in combination with a white diffuse dielectric back reflector. The sensitivity of the ZnO towards the acidic aqueous environment from which we draw the spheres prevented the direct organization of the colloidal crystal on the cell surface. To overcome this issue, we developed a transfer printing technique based on the work of Yang [28] (Fig. 5a). The colloidal crystals were fabricated as previously described, on a glass slide. For each cell, a poly(dimethylsiloxane) (PDMS) stamp was pressed into the colloidal array, peeled away, then pressed onto the device surface, which was first spin-coated with 15–20 nm of poly(vinyl alcohol) (PVA) from an aqueous solution containing 5% gluteraldehyde. The cells were heated to 100 °C under argon for 2 h, to crosslink the polymer around (and to) the sphere base. Despite the fact that the nominal PVA thickness is only 2–3% of the sphere diameter, the colloidal crystals were effectively transferred to the device surface with high fidelity and good yield. We attribute this robust adhesion to the fact that gluteraldehyde can couple to both the hydroxyl groups of the polymer as well as the amines on the sphere surface, enabling both polymer/polymer and polymer/sphere crosslinking (Fig. 5a). Generally, it is crucial that the PVA spacer remain optically thin, as an adjacent material can perturb the resonant modes and parasitically confine light.

The performance of the solar cell with and without the sphere array is plotted in Fig. 5c and d. A relative enhancement of 1.8% is seen for the highest efficiency, which reaches 11.1%. Enhancement in EQE occurs around 450 and 650 nm resulting in a short circuit current increase of 1.8% from 15.9 to 16.2 mA cm^{-2}. Fill factor and open circuit voltage remain the same at about 75% and 910 mV, respectively. Due to its structural complexity, we did not simulate the full cell architecture. While PC mode

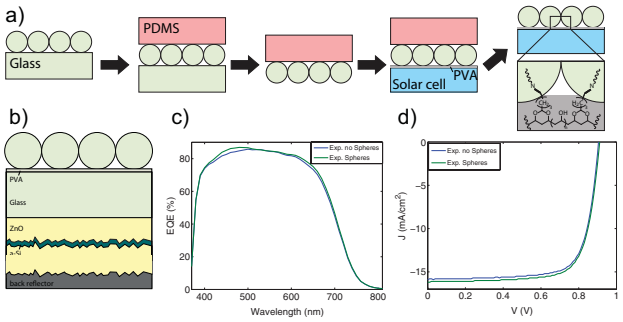

Figure 5 (online color at: www.pss-a.com) Transfer printing of colloidal monolayers onto high efficiency solar cells. (a) Fabrication steps of the transfer printing technique used to coat the solar cell with nanospheres. A PDMS stamp is pressed into the 2D colloidal crystal formed on a glass slide by Langmuir–Blodgett deposition. The PDMS stamp is then peeled away to ink the stamp with spheres. PDMS and spheres are pressed onto the solar cell coated with 15 nm PVA and heated for 2 h at 100 °C to crosslink PVA. Finally, the PDMS stamp is peeled away to leave a printed colloidal crystal embedded in the cross-linked PVA film. The inset depicts possible bonding arrangements between the aminated sphere array and glutaraldehyde crosslinked PVA network. (b) 2D cross section of the rough a-Si:H solar cell. (c) Measured EQE and (d) current–voltage with and without spheres.

resonances are not directly observed for this cell architecture, the 2D colloidal crystal nevertheless proves an effective antireflection coating. We attribute the enhancement here to the graded index provided by the sphere geometry [29], which is supported by transfer matrix simulations (see Fig. S5, Supporting Information). These results contrast with the flat cell, where the spectral features associated with near field coupling between the PC modes and the active layer could not be accounted for by this simple graded index model. While the resonant features are not observed in the EQE spectrum of the absorber layer with the colloidal crystal in the far field, this example demonstrates that our approach can be combined with other state-of-the-art light-trapping techniques, specifically active layer texturing.

5 Conclusions We have experimentally demonstrated efficiency enhancement of thin-film a-Si:H solar cells using PC modes of resonant dielectric structures. This type of light trapping could enable one to reduce the thickness of the active layer, resulting in electrical improvement and cost reduction. When the resonant structure is near the active absorbing layer, the proposed mechanism of coupling through PC resonances is verified by measurements of silica nanosphere arrays on a flat a-Si:H solar cell. Due to the fabricated geometry of our resonant dielectric structures, the relative enhancement of absorption is largely insensitive to the incident angle of the sunlight. This is important for many PV applications, such as residential installations, where tracking is prohibitive and diffuse light accounts for a significant fraction of the available solar energy. This type of modification can be employed after device fabrication, and combined with other light trapping schemes to further enhance PV performance. We are also considering higher index materials like TiO_2 spheres. Such higher index material can be embedded in EVA [23], which is commonly used for solar cell encapsulation. We have developed a method that enables the transfer of high fidelity colloidal crystals to device surfaces, using an optically thin and chemically robust adhesion layer. Finally, we have demonstrated that 2D colloidal crystals can also improve the efficiency of ultra-high efficiency amorphous silicon solar cells, which already incorporate random texturing as a light-trapping element. Our methods are relevant to improving a variety of other devices, including photodetectors, LEDs, photoelectrochemical cells, bioreactors, and sensors. Resonant dielectric structures offer a versatile light-trapping solution, which is simple to implement and has significant potential to improve solar energy conversion.

Supporting information (see online at: www.pss-a.com) Silica nanosphere functionalization, Langmuir–Blodgett deposition (movie), transfer printing preparation, effective index model, optical measurement on bare crystalline silicon, graded-index model: transfer matrix simulations, angle measurements on a flat solar cell, optical parameters, electrical measurement, and electrical parameters.

Acknowledgements The authors wish to thank A. J. Leenheer, A. Mihi, P. V. Braun, M. Charrière, and K. Söderström for useful technical input. The work at Caltech was supported by the "Light–Material Interactions in Energy Conversion" Energy Frontier Research Center funded by the U.S. Department of Energy, Office of Science, Office of Basic Energy Sciences under Award Number DE-SC0001293. The work at EPFL was supported by the Swiss Federal Energy Office. RAW thanks the Resnick Sustainability Institute for a graduate fellowship.

References

[1] A. V. Shah, H. Schade, M. Vanecek, J. Meier, E. Vallat-Sauvain, N. Wyrsch, U. Kroll, C. Droz, and J. Bailat, Progr. Photovolt. Res. Appl. **12**, 113–142 (2004).
[2] E. Yablonovitch and G. D. Cody, IEEE Trans. Electron Devices **29**, 300–305 (1982).
[3] J. Zhao and M. A. Green, IEEE Trans. Electron Devices **38**, 1925–1934 (1991).
[4] C.-M. Hsu, C. Battaglia, C. Pahud, Z. Ruan, F.-J. Haug, S. Fan, C. Ballif, and Y. Cui, Adv. Energy Mater. **2**, 628–633 (2012).
[5] H. A. Atwater and A. Polman, Nature Mater. **9**, 205–213 (2010).
[6] K. R. Catchpole and A. Polman, Opt. Express **16**, 21793–21800 (2008).
[7] X. Li, N. P. Hylton, V. Giannini, K.-H. Lee, N. J. Ekins-Daukes, and S. A. Maier, Opt. Express **19**, A888–A896 (2011).
[8] R. A. Pala, J. White, E. Barnard, J. Liu, and M. L. Brongersma, Adv. Mater. **21**, 3504–3509 (2009).
[9] P. Bermel, C. Luo, L. Zeng, L. C. Kimerling, and J. D. Joannopoulos, Opt. Express **15**, 16986–17000 (2007).
[10] S. A. Mann, R. R. Grote, R. M. Osgood, and J. A. Schuller, Opt. Express **19**, 25729–25740 (2011).

[11] P. Spinelli, M. A. Verschuuren, and A. Polman, Nature Commun. **3**, 692 (2012).
[12] M. Kroll, S. Fahr, C. Helgert, C. Rockstuhl, F. Lederer, and T. Pertsch, Phys. Status Solidi A **205**, 2777–2795 (2008).
[13] Y. Yao, J. Yao, V. K. Narasimhan, Z. Ruan, C. Xie, S. Fan, and Y. Cui, Nat. Commun. **3**, 664 (2012).
[14] J. Grandidier, D. M. Callahan, J. N. Munday, and H. A. Atwater, Adv. Mater. **23**, 1272–1276 (2011).
[15] J. Grandidier, D. M. Callahan, J. N. Munday, and H. A. Atwater, IEEE J. Photovoltaics **2**, 123–128 (2012).
[16] J. Grandidier, M. G. Deceglie, D. M. Callahan, and H. A. Atwater, J. Photon. Energy **2**, 024502 (2012).
[17] C. Battaglia, C.-M. Hsu, K. Söderström, J. Escarré, F.-J. Haug, M. Charrière, M. Boccard, M. Despeisse, D. T. L. Alexander, M. Cantoni, Y. Cui, and C. Ballif, ACS Nano **6**, 2790–2797 (2012).
[18] R. M. Cole, Y. Sugawara, J. J. Baumberg, S. Mahajan, M. Abdelsalam, and P. N. Bartlett, Phys. Rev. Lett. **97**, 137401 (2006).
[19] A. Mihi, C. Zhang, and P. V. Braun, Angew. Chem. Int. Ed. **50**, 5712–5715 (2011).
[20] P. Jiang, J. F. Bertone, K. S. Hwang, and V. L. Colvin, Chem. Mater. **11**, 2132–2140 (1999).
[21] C.-M. Hsu, S. T. Connor, M. X. Tang, and Y. Cui, Appl. Phys. Lett. **93**, 133109-3. (2008).
[22] J. Zhu, Z. Yu, S. Fan, and Y. Cui, Mater. Sci. Eng. R **70**, 330–340 (2010).
[23] J. Grandidier, D. M. Callahan, and H. A. Atwater, Configuration optimization of a nanosphere array on top of a thin film solar cell, in: PVSC (2012).
[24] M. G. Deceglie, V. E. Ferry, A. P. Alivisatos, and H. A. Atwater, Nano Lett. **12**, 2894–2900 (2012).
[25] M. López-García, J. F. Galisteo-López, C. López, and A. García-Martín, Phys. Rev. B **85**, 235145 (2012).
[26] B. Marion, B. Kroposki, K. Emery, J. del Cueto, D. Myers, and C. Osterwald, Validation of a photovoltaic module energy ratings procedure at NREL, Technical report NREL/TP-520-26909 (1999).
[27] C. Battaglia, J. Escarre, K. Soderstrom, M. Charriere, M. Despeisse, F.-J. Haug, and C. Ballif, Nature Photon. **5**, 535–538 (2011).
[28] X. Yan, J. Yao, G. Lu, X. Chen, K. Zhang, and B. Yang, J. Am. Chem. Soc. **126**, 10510–10511 (2004).
[29] C.-Y. Fang, Y.-L. Liu, Y.-C. Lee, H.-L. Chen, D.-H. Wan, and C.-C. Yu, Adv. Funct. Mater., DOI: 10.1002/adfm.201201949 (2012).

